



**Activation of Pannexin-1 Hemichannels Augments
Aberrant Bursting in the Hippocampus**

Roger J. Thompson, *et al.*
Science **322**, 1555 (2008);
DOI: 10.1126/science.1165209

**The following resources related to this article are available online at
www.sciencemag.org (this information is current as of January 19, 2009):**

Updated information and services, including high-resolution figures, can be found in the online version of this article at:

<http://www.sciencemag.org/cgi/content/full/322/5907/1555>

Supporting Online Material can be found at:

<http://www.sciencemag.org/cgi/content/full/322/5907/1555/DC1>

This article **cites 21 articles**, 10 of which can be accessed for free:

<http://www.sciencemag.org/cgi/content/full/322/5907/1555#otherarticles>

This article appears in the following **subject collections**:

Neuroscience

<http://www.sciencemag.org/cgi/collection/neuroscience>

Information about obtaining **reprints** of this article or about obtaining **permission to reproduce this article** in whole or in part can be found at:

<http://www.sciencemag.org/about/permissions.dtl>

5. C. Giaume, K. D. McCarthy, *Trends Neurosci.* **19**, 319 (1996).
6. J. I. Nagy, J. E. Rash, *Brain Res. Brain Res. Rev.* **32**, 29 (2000).
7. J. I. Nagy, D. Patel, P. A. Y. Ochalski, G. L. Stelmack, *Neuroscience* **88**, 447 (1999).
8. Materials and methods are available as supporting material on *Science Online*.
9. L. Pellerin, P. Magistretti, *Proc. Natl. Acad. Sci. U.S.A.* **91**, 10625 (1994).
10. K. Matthias *et al.*, *J. Neurosci.* **23**, 1750 (2003).
11. A. Wallrapp, B. Odermatt, K. Willecke, C. Steinhäuser, *Glia* **48**, 36 (2004).
12. D. C. Spray, Z. C. Ye, B. R. Ransom, *Glia* **54**, 758 (2006).
13. G. F. Tian *et al.*, *Nat. Med.* **11**, 973 (2005).
14. M. Garriga-Canut *et al.*, *Nat. Neurosci.* **9**, 1382 (2006).
15. M. L. Cotrina *et al.*, *J. Neurosci.* **18**, 2520 (1998).
16. We thank P. Ezan for technical assistance and R. Nicoll, G. Bonvento, J. Deitmer, and P. Magistretti for helpful discussions. This work was supported by grants from the Human Frontier Science Program Organization (Career Development Award) and Agence Nationale de la Recherche (Programme Jeunes chercheurs) to N.R.; from INSERM to N.R., A.K., and C.G.; from the German

Research Association (SFB 645, B3) to K.W.; and from International Brain Research Organization to V.A. N.R. dedicates this work to her daughter Angela.

Supporting Online Material

www.sciencemag.org/cgi/content/full/322/5907/1551/DC1
Materials and Methods
SOM Text
Figs. S1 to S6
References

31 July 2008; accepted 29 October 2008
10.1126/science.1164022

Activation of Pannexin-1 Hemichannels Augments Aberrant Bursting in the Hippocampus

Roger J. Thompson,^{1,†} Michael F. Jackson,² Michelle E. Olah,² Ravi L. Rungta,¹ Dustin J. Hines,¹ Michael A. Beazely,² John F. MacDonald,² Brian A. MacVicar^{1†}

Pannexin-1 (Px1) is expressed at postsynaptic sites in pyramidal neurons, suggesting that these hemichannels contribute to dendritic signals associated with synaptic function. We found that, in pyramidal neurons, *N*-methyl-D-aspartate receptor (NMDAR) activation induced a secondary prolonged current and dye flux that were blocked with a specific inhibitory peptide against Px1 hemichannels; knockdown of Px1 by RNA interference blocked the current in cultured neurons. Enhancing endogenous NMDAR activation in brain slices by removing external magnesium ions (Mg²⁺) triggered epileptiform activity, which had decreased spike amplitude and prolonged interburst interval during application of the Px1 hemichannel blocking peptide. We conclude that Px1 hemichannel opening is triggered by NMDAR stimulation and can contribute to epileptiform seizure activity.

Hemichannels are formed by pannexin or connexin proteins and mediate large ionic currents and the passage of small molecules (<1 kD) across plasma membranes. Pannexin-1 (Px1) forms hemichannels in a number of cell types and can be opened by ischemic-like conditions in pyramidal neurons (1) or purinergic receptor stimulation in red blood cells (2). Px1 has been observed at the postsynaptic density by electron microscopy and colocalization with postsynaptic density protein 95 (PSD95) (3); therefore, we hypothesized that Px1 hemichannels may have an undiscovered function at postsynaptic sites. Glutamate mediates excitatory synaptic communication via activation of fast AMPA/kainate and slower *N*-methyl-D-aspartate receptors (NMDARs). We investigated the possibility that NMDAR activation opens Px1 hemichannels because of reports that NMDARs lead to a prolonged but unidentified secondary inward current (4–6).

Under conditions in which voltage-dependent ion channels were blocked, we recorded NMDAR secondary currents (I_{2nd}) from acutely isolated hippocampal neurons with whole-cell patch clamp and activated them by either repeated (10-s duration at 1-min intervals) (Fig. 1A) or continuous (5 to 15 min) 100 μ M NMDA with concomitant voltage commands from -80 to $+80$ mV (Figs. 1D and 2) (7). I_{2nd} was evident as an increase in holding current (Fig. 1A, downward shift in middle trace) and was secondary to the NMDAR because it persisted after washout of the agonist (Fig. 1A). Furthermore, I_{2nd} was blocked by 50 μ M carbenoxolone (Cbx) (Fig. 1, A to C), an inhibitor of gap junctions and hemichannels (8). We tested a selective small peptide inhibitor of Px1, ¹⁰panx (100 μ M; WRQAAFVDSY) (9, 10), that blocked I_{2nd} [Fig. 1, B and C; $P < 0.05$, analysis of variance (ANOVA)], whereas a scrambled version, ^{sc}panx (FSVYWAQADR), was ineffective (Fig. 1C; Px1 group, $P > 0.05$, ANOVA). Block of the NMDAR ligand-gated currents with 1 mM kynurenic acid prevented activation of I_{2nd} (fig. S1). Furthermore, the NMDAR currents were not directly affected by Cbx or ¹⁰panx as determined by applying these blockers before activation of I_{2nd} (Fig. 1C; $P > 0.05$, ANOVA). Similar to Px1 activation by ischemia (1), I_{2nd} had a linear current-voltage relation (Fig. 1B). Although this differs from some Px1 expression systems (8, 9, 11), it is

similar to the “large-conductance” mode of P2X7 in human embryonic kidney cells (12), which may be mediated by Px1 (9).

The pores of hemichannels are large enough to permit flux of large molecules (13), making dye flux a powerful tool for identifying the involvement of Px1. If Px1 mediates I_{2nd} , then NMDAR activation should evoke efflux of calcein (a non-reactive fluorescent indicator) from hippocampal neurons. We loaded acutely isolated hippocampal neurons with calcein red/orange and with a calcium indicator (Fluo-4 or Fluo-4FF) to monitor activation of the NMDAR. NMDA (100 μ M), applied for 5 to 10 min to acutely isolated hippocampal neurons in 0 Mg²⁺ solution to enhance NMDA currents without requiring simultaneous membrane depolarization, evoked rapid rises in intracellular calcium concentration ([Ca]_i) that persisted after washout of the agonist. Calcein red/orange efflux from single neurons occurred with a delay (average 7.9 ± 1.6 min; $n = 7$ number of cells) after the NMDA-induced [Ca]_i rise, (Fig. 1, D to F). Dye efflux was blocked when 100 μ M ¹⁰panx was present (Fig. 1, E and F) (1, 14).

By using RNA interference of Px1 in cultured hippocampal neurons, we next confirmed that the NMDAR-evoked I_{2nd} was due to Px1 hemichannels. We first demonstrated that short hairpin RNA (shRNA) delivered to cultured hippocampal neurons via lentivirus (see supporting online material) reduced Px1 levels. Infection of cultured neurons with green fluorescent protein (GFP) and the shRNA vector was achieved at >80% efficiency and with minimal infection of non-neuronal cells. This resulted in knockdown of the Px1 protein in the total culture to $43 \pm 10\%$ of control ($P < 0.05$; ANOVA; $n = 4$), as determined by Western blot analysis with an antibody against a C-terminal region of Px1 (Fig. 2A) (15). The remaining 43% may be due to expression of Px1 in other cell types in the culture, such as astrocytes (16), and incomplete efficacy of the shRNA. We then used sister cultures to test whether the NMDAR I_{2nd} was reduced after shRNA knockdown of Px1. Intensely GFP-positive (that is, shRNA-expressing) neurons were patch-clamped, and NMDA (100 μ M) was applied for 2 to 10 min, which activated I_{2nd} (Fig. 2, B and D). Maximal activation was achieved after 5 min of agonist application (Fig. 2, B and D). The Px1 inhibitor, ¹⁰panx (100 μ M) blocked activation of I_{2nd} (Fig. 2, C and D), and shRNA-expressing neurons had significantly reduced I_{2nd} (by >70%),

¹Department of Psychiatry and Brain Research Centre, University of British Columbia, 2211 Wesbrook Mall, Vancouver, BC V6T 2B5, Canada. ²Robarts Research Institute, University of Western Ontario, London, ON N6A 5K8, Canada.

*Present address: Department of Cell Biology and Anatomy and Hotchkiss Brain Institute, University of Calgary, 3330 Hospital Drive Northwest, Calgary, AB T2N 4N1, Canada.

†To whom correspondence should be addressed. E-mail: rj.thompson@ucalgary.ca (R.J.T.); bmacvicar@brain.ubc.ca (B.A.M.)

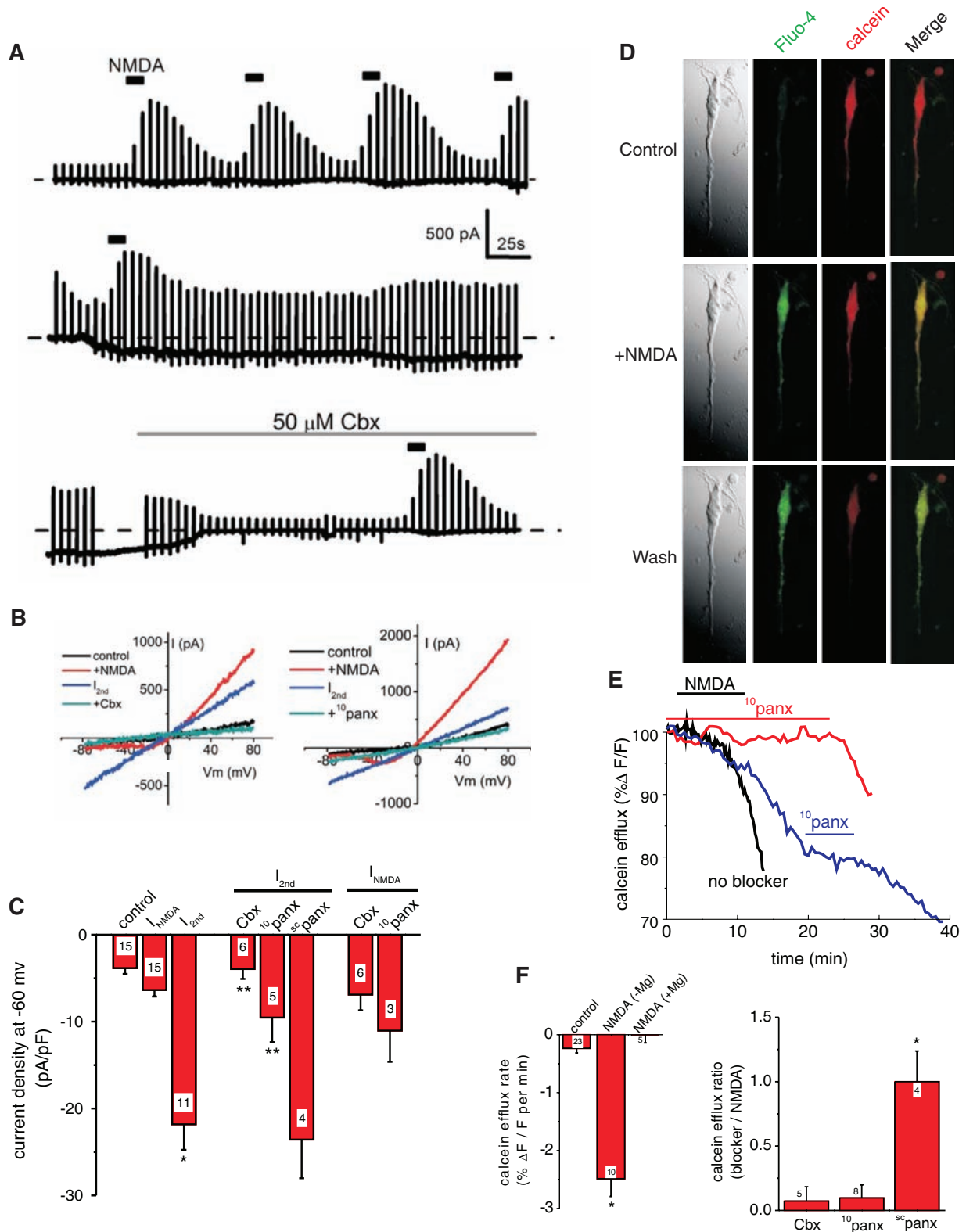


Fig. 1. NMDAR activation opens Px1 hemichannels in hippocampal neurons. **(A)** Continuous voltage-clamp recording ($V_m = -60$ mV) from a neuron exposed to repetitive 10 s applications of 100 μ M NMDA (bars). I_{2nd} (downward shift in middle trace) was blocked by carbenoxolone (Cbx). Each spike is an applied voltage ramp from -80 to $+80$ mV. **(B)** Current-voltage plots of applied voltage ramps. I_{2nd} was inhibited by Cbx and a peptide inhibitor of Px1, 10 panx. **(C)** Quantification of NMDAR current (I_{NMDA}) and I_{2nd} recorded from isolated hippocampal neurons. Activation of I_{2nd} was significantly (asterisk) larger than

control and blocked (two asterisks) by Cbx or 10 panx, but not scrambled 10 panx (sc panx). I_{NMDA} (before I_{2nd} activation) was not affected by Cbx or 10 panx. Error bars indicate SEM. **(D)** Acutely isolated hippocampal neuron loaded with Fluo-4 and calcein red/orange. Calcium remained elevated and calcein red/orange efflux occurred after NMDA exposure. **(E)** Efflux was blocked by 10 panx when applied concomitantly with NMDA (red) or once dye loss had begun (blue), as quantified in **(F)**. Cbx, 10 panx, and Mg^{2+} prevented efflux. In the right graph of **(F)**, a value of 1.0 indicated no effect of the blocker.

but those infected with a scrambled shRNA were not different from control (Fig. 2, A, C, and D). The residual currents that remained (<30% of control) in the shRNA-infected individual neurons (Fig. 2, C and D) were probably due to incomplete block of Px1 expression by shRNA vectors, but the possibility that other cation channels make a minor contribution cannot be excluded.

The activation of Px1 hemichannels by NMDAR stimulation and the reported expression of these hemichannels at postsynaptic sites (3) raised the interesting possibility that Px1 can be opened by synaptically released glutamate. Hippocampal slices were thus exposed to low Mg^{2+}

concentrations plus 5 mM KCl to potentiate NMDAR currents in intact tissue. These slices displayed a pattern of rhythmic epileptiform-like bursting called interictal spiking—a correlate to repetitive bursting electroencephalography rhythms observed in epilepsy patients (17). We confirmed that the initiation of interictal bursts in brain slices was triggered by synaptic NMDAR activation, as previously reported (18), by blocking the induction of bursting with NMDAR antagonists. We tested whether Px1 hemichannels are opened by synaptic activity (during 0 Mg^{2+} triggered bursting) via measuring dye uptake by neurons through Px1 and the electrophysiological contribution of Px1 to interictal discharges.

Exposure of 400- μ m-thick rodent brain slices to nominally Mg^{2+} -free solutions induced uptake of a fluorescent dye, sulforhodamine 101 (SR101), into neurons in the CA1 region of the hippocampus (Fig. 3). SR101 is normally a selective marker of astrocytes and is excluded from neurons (Fig. 3A) (19). However, in our previous work, SR101 influx into cortical neurons occurred during ischemia and was indicative of Px1 opening (1). In 0 Mg^{2+} exposed hippocampal slices, SR101 influx into CA1 hippocampal neurons was observed (Fig. 3A), and dye influx was blocked by 10 panx or pre-treatment with 50 μ M APV [(2R)-amino-5-phosphonovaleric acid], an NMDAR antagonist (Fig. 3).

Fig. 2. NMDAR I_{2nd} block by RNA interference of Px1. **(A)** Cultured hippocampal neurons infected with GFP and shRNA against Px1 had significant ($P < 0.05$, ANOVA) knockdown of the hemichannel, as assayed by Western blot. siRNA, small interfering RNA. Error bars indicate SEM. **(B)** Time-dependent activation of the I_{2nd} on exposure of cultures to NMDA (arrow) for the time indicated. **(C)** 10 panx blocked the I_{2nd} activated by 5-min NMDA. Knockdown of Px1 with shRNA, but not a scrambled shRNA (sc), blocked the I_{2nd} recorded from GFP-positive neurons. **(D)** Quantification of I_{2nd} (at -60 mV) of cultured hippocampal neurons exposed to NMDA. All statistical comparisons were made to the current amplitude for a 5-min exposure to NMDA (ANOVA; $P < 0.05$). The asterisk indicates a significant difference from the 5-min NMDA application.

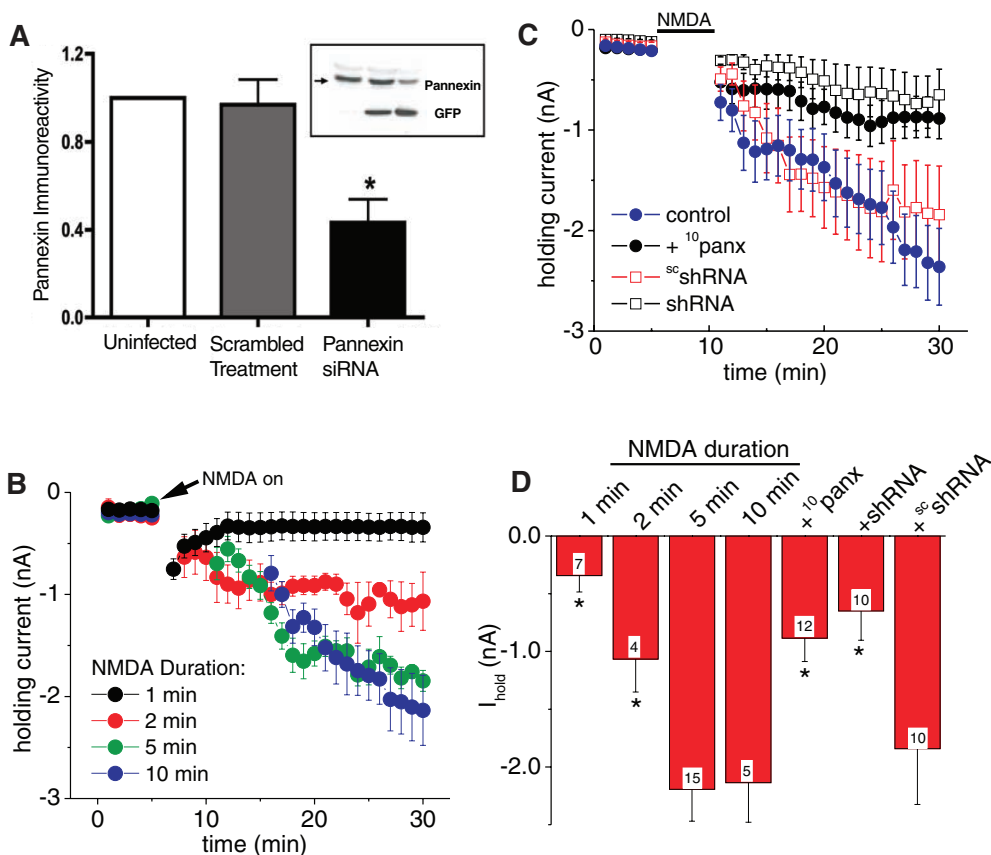
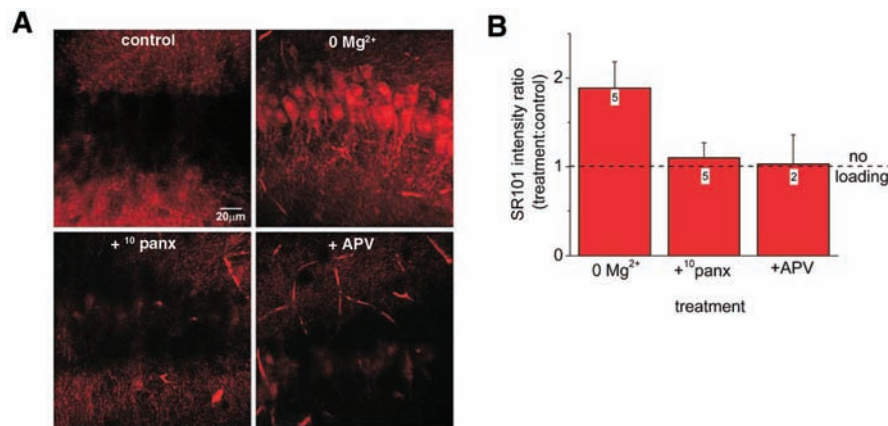


Fig. 3. NMDAR potentiation in hippocampal brain slices opens Px1. **(A)** CA1 region of the hippocampus is shown 75 μ m deep into 400- μ m slices. The red fluorescent dye SR101 is excluded from neurons (control). A 1-hour exposure to Mg^{2+} -free (+5 mM KCl) bathing solution evoked dye uptake that was blocked by 10 panx or APV. **(B)** Dye uptake, expressed as fluorescence intensity after treatment with 0 Mg^{2+} , 0 Mg^{2+} + 10 panx, or 0 Mg^{2+} + APV as the ratio of SR101 intensity to that in control slices. Error bars indicate SEM.



To further test the involvement of Px1 in hippocampal synaptic function, we recorded the extracellular field potentials that spontaneously occur after a ~1-hr exposure of hippocampal slices to 0 Mg^{2+} plus 5 mM KCl bathing solutions. These interictal bursts (Fig. 4A) in the CA1 region occurred at 0.6 ± 0.2 Hz ($n = 5$ slices), and the addition of $^{10}panx$ reduced the interburst frequency by $24 \pm 6\%$, which recovered to $103 \pm 8\%$ of control upon washout of the blocking peptide (Fig. 4, A, B, and D). Block of Px1 during interictal bursting also decreased the mean amplitude of spikes within a burst by $34 \pm 6\%$ ($P < 0.05$ by ANOVA), with recovery to $73 \pm 12\%$ of control ($n = 5$) (Fig. 4, A to C). When $^{10}panx$ was coapplied initially with the 0 Mg^{2+} solutions, interictal bursting still occurred, but the amplitude and frequency increased after

washout of the peptide (fig. S2). The effect of Px1 block on spike properties and bursting in the epileptic-like hippocampus was not attributable to nonspecific inhibition of fast (AMPA receptor-mediated) synaptic transmission because $^{10}panx$ did not affect field potentials evoked by stimulation of the Schaeffer collateral pathway in the presence of 2 mM extracellular Mg^{2+} (Fig. 4D).

The data presented here demonstrate that Px1 hemichannels are activated by NMDARs and contribute to postsynaptic responses in the hippocampus during seizure-like activity. This result is consistent with Px1 providing a tonic depolarizing current in dendrites during intense NMDAR activity. This could be initiated either synaptically or extra-synaptically, but the presence of Px1 in the postsynaptic density suggests that synaptic

activation of Px1 is probably involved. We have determined that Px1 hemichannels constitute a major portion of the NMDAR-evoked I_{2nd} , which can lead to Ca^{2+} deregulation in hippocampal pyramidal neurons and possibly to the establishment of acquired epilepsy (4–6, 20). It has been suggested that interneuronal gap junctions contribute to epileptogenesis in the hippocampus (21). It will be interesting to determine the relation between these junctions and Px1 hemichannel activation during seizures.

What is the mechanism that links NMDAR to Px1 activation? Surprisingly, it does not appear to involve increased intracellular Ca^{2+} , because altering neuronal Ca^{2+} buffering did not affect Px1 opening (fig. S3). The mechanism may, however, involve intracellular adenosine triphosphate (ATP) depletion during NMDAR activation (22), be-

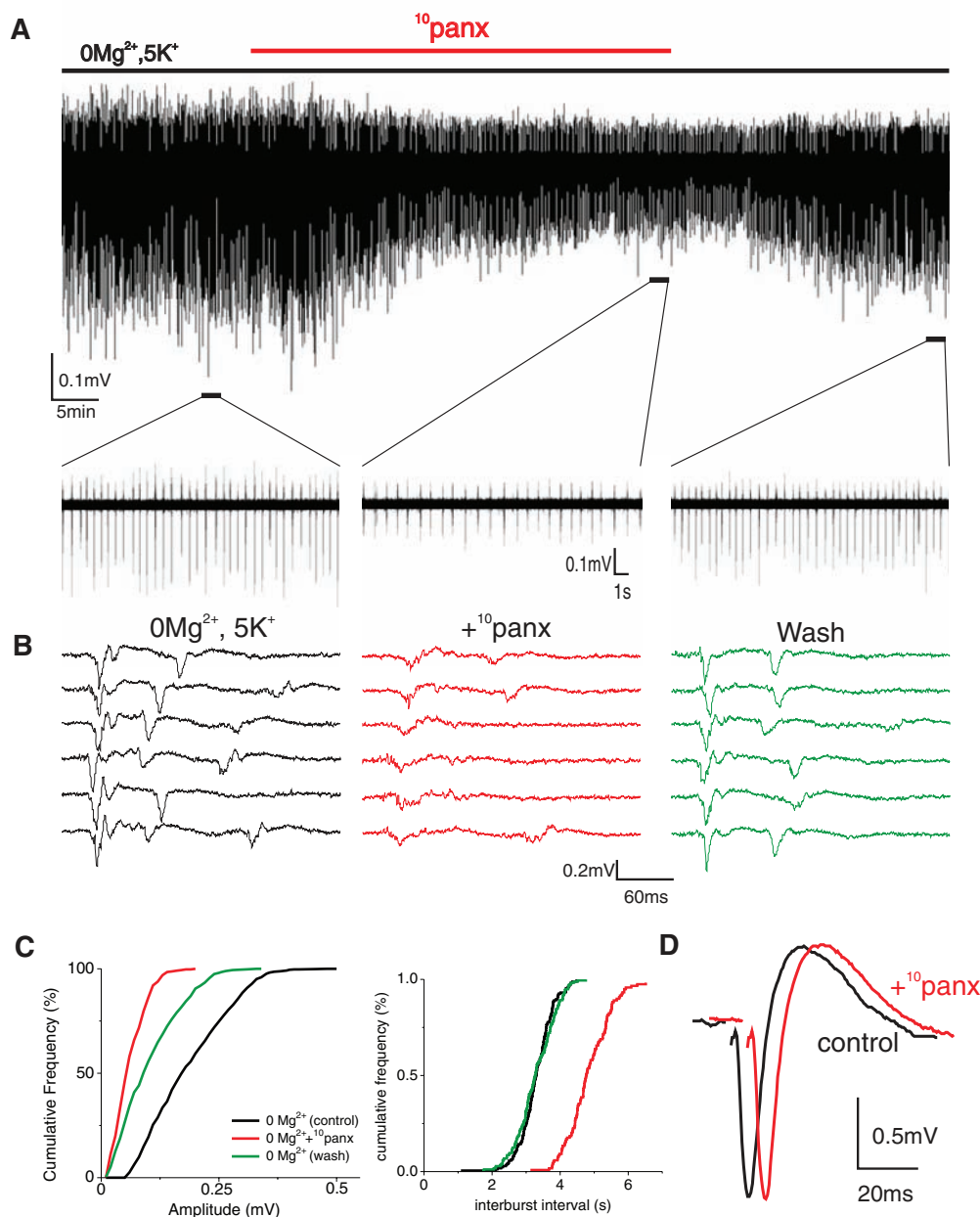


Fig. 4. Px1 block alters bursting properties of hippocampal neurons during seizure-like events. **(A)** Interictal spiking, induced by low Mg^{2+} concentration plus 5 mM KCl, was affected by $^{10}panx$. Decreases in burst frequency and amplitude are evident. **(B)** Expanded bursts demonstrated significant (ANOVA; $P < 0.05$) alteration of electro-physiological properties by Px1 inhibition. **(C)** Cumulative frequency plots of spike amplitude and interburst interval showing decreased spike amplitude and a longer interval between bursts when Px1 was blocked. **(D)** Evoked potentials by stimulation of Schaeffer collaterals in the presence of 2 mM extracellular Mg^{2+} to block NMDARs, demonstrating that $^{10}panx$ did not directly block fast synaptic transmission via AMPA receptors.

cause intracellular perfusion with 4 mM MgATP significantly protected against Pxl activation; current density was -30.2 ± 8.6 pA/pF ($n = 3$) with 1 mM MgATP and -9.4 ± 3.7 pA/pF ($n = 5$) with 4 mM MgATP. We recently reported that Pxl is opened by ischemia (1) and that the timing of this opening appears to follow the anoxic depolarization (23) in a manner analogous to Pxl activation after NMDAR stimulation. Therefore, Pxl not only appears to be involved in neuronal dysfunction during ischemia but also plays a role in the potentiation of seizure-like activity. These unique ion channels should therefore be considered important targets for the treatment of neurological disorders such as epilepsy and stroke.

References and Notes

1. R. J. Thompson, N. Zhou, B. A. MacVicar, *Science* **312**, 924 (2006).
2. S. Locovei, L. Bao, G. Dahl, *Proc. Natl. Acad. Sci. U.S.A.* **103**, 7655 (2006).
3. G. Zoidl et al., *Neuroscience* **146**, 9 (2007).

4. Q. X. Chen, K. L. Perkins, D. W. Choi, R. K. S. Wong, *J. Neurosci.* **17**, 4032 (1997).
5. J. A. Connor, R. J. Cormier, *J. Neurophysiol.* **83**, 90 (2000).
6. M. Tymianski, M. P. Charlton, P. L. Carlen, C. H. Tator, *J. Neurosci.* **13**, 2085 (1993).
7. Materials and methods are available as supporting material on Science Online.
8. R. Bruzzone, S. G. Hormuzdi, M. T. Barbe, A. Herb, H. Monyer, *Proc. Natl. Acad. Sci. U.S.A.* **100**, 13644 (2003).
9. P. Pelegrin, A. Surprenant, *EMBO J.* **25**, 5071 (2006).
10. Single-letter abbreviations for the amino acid residues are as follows: A, Ala; C, Cys; D, Asp; E, Glu; F, Phe; G, Gly; H, His; I, Ile; K, Lys; L, Leu; M, Met; N, Asn; P, Pro; Q, Gln; R, Arg; S, Ser; T, Thr; V, Val; W, Trp; and Y, Tyr.
11. L. Bao, S. Locovei, G. Dahl, *FEBS Lett.* **572**, 65 (2004).
12. C. Virginio, A. MacKenzie, R. A. North, A. Surprenant, *J. Physiol.* **519**, 335 (1999).
13. D. C. Spray, Z.-C. Ye, B. R. Ransom, *Glia* **54**, 758 (2006).
14. P. Pelegrin, A. M. Surprenant, *EMBO J.* **25**, 5071 (2007).
15. S. Penuela et al., *J. Cell Sci.* **120**, 3772 (2006).
16. Y. Huang, J. B. Grinspan, C. K. Abrams, K. S. Scherer, *Glia* **55**, 46 (2007).
17. H. Walthers, J. D. C. Lambert, R. S. G. Jones, U. Heinemann, B. Hamon, *Neurosci. Lett.* **69**, 156 (1986).
18. J. P. Dreier, U. Heinemann, *Neurosci. Lett.* **119**, 68 (1990).

19. A. Nimmerjahn, F. Kirchhoff, J. N. D. Kerr, F. Helmchen, *Nat. Methods* **1**, 31 (2004).
20. E. A. Waxman, D. R. Lynch, *Neuroscientist* **11**, 37 (2005).
21. M. V. L. Bennett, A. Pereda, *Brain Cell Biol.* **35**, 5 (2007).
22. T. A. Vander Jagt, J. A. Connor, C. W. Shuttleworth, *J. Neurosci.* **28**, 5029 (2008).
23. T. H. Murphy, P. Li, K. Betts, R. Liu, *J. Neurosci.* **28**, 1756 (2008).
24. This work was supported by grants to B.A.M. from the Heart and Stroke Foundation of British Columbia, to B.A.M. or J.F.M. (15514) from the Canadian Institutes of Health Research, and by a grant from the Canadian Stroke Network to B.A.M., J.F.M., and R.J.T. B.A.M. holds a Canada Research Chair (Tier 1) in Neuroscience. The authors kindly acknowledge Y. T. Wang for critical reading of the manuscript and S. Panuela and D. Laird for generously providing the anti-Pxl antibody.

Supporting Online Material

www.sciencemag.org/cgi/content/full/322/5907/1555/DC1
Materials and Methods
Figs. S1 to S3
References

27 August 2008; accepted 29 October 2008
10.1126/science.1165209

Centromere-Associated Female Meiotic Drive Entails Male Fitness Costs in Monkeyflowers

Lila Fishman* and Arpiar Saunders†

Female meiotic drive, in which paired chromosomes compete for access to the egg, is a potentially powerful but rarely documented evolutionary force. In interspecific monkeyflower (*Mimulus*) hybrids, a driving *M. guttatus* allele (*D*) exhibits a 98:2 transmission advantage via female meiosis. We show that extreme interspecific drive is most likely caused by divergence in centromere-associated repeat domains and document cytogenetic and functional polymorphism for drive within a population of *M. guttatus*. In conspecific crosses, *D* had a 58:42 transmission advantage over nondriving alternative alleles. However, individuals homozygous for the driving allele suffered reduced pollen viability. These fitness effects and molecular population genetic data suggest that balancing selection prevents the fixation or loss of *D* and that selfish chromosomal transmission may affect both individual fitness and population genetic load.

In the female meioses of both plants and animals, all but one of the meiotic products generally degenerate (1). This asymmetry of cell fate can allow homologous chromosomes to compete for inclusion in the single surviving egg or megaspore, a process termed “female meiotic drive” (1–4). Female meiotic drive may explain the rapid diversification of centromeres, the DNA-protein complexes that mediate chromosomal segregation (5), and may promote speciation through the evolution of hybrid incompatibilities (5) and karyotypic rearrangements (6). Because nondisjunction during chromosomal competition can cause infertility (2, 5), female meiotic drive may also contribute to genetic variation for reproduc-

tive fitness within populations (7), a central issue in evolutionary biology (8–12) and human health. Despite its potential importance as an evolutionary force, little is known about female meiotic drive in natural populations.

The female meiotic-drive locus in *Mimulus* (*D*) exhibits extreme non-Mendelian segregation through female meiosis in hybrids between *M. guttatus* (IM62 inbred line) and its close relative *M. nasutus* (SF inbred line), which is predominantly self-fertilizing (13, 14). As seed parents, interspecific heterozygotes transmit >98% *M. guttatus* (IM62) alleles at markers tightly linked to *D*, and there is no evidence of postmeiotic mechanisms of transmission ratio distortion (13). Near-complete transmission bias via female meiosis suggests that *D* is the functional centromere of the chromosome corresponding to the linkage group [linkage group 11 (LG11)] on which it is located (13), because only the centromere (and linked loci) can attain >83.3% transmission via

female drive (15). To test this inference, we cytogenetically mapped *D* in *M. guttatus*, *M. nasutus*, and interspecific hybrids (Fig. 1) (SOM text). Because plant centromeres generally consist of megabases of tandemly repetitive DNA with individual repeats 150 to 1000 base pairs (bp) in length (16, 17), we searched the *M. guttatus* (IM62 line) 6× draft whole-genome sequence [Mimulus Genome Project, U.S. Department of Energy (DOE) Joint Genome Institute] for repeats with those features. A probe for the most common class of repeat found, 728 bp in length (Cent728; fig. S1), hybridized to a single narrow band near the center of each IM62 metaphase chromosome (Fig. 1A and fig. S2A). However, a single pair of homologous chromosomes exhibited two unusually large regions of hybridization (arrows; Fig. 1A and fig. S2A). A probe for the *CycA* genetic marker tightly linked to *D* (13) localized between the large Cent728 arrays on this chromosome (Fig. 1B and fig. S2B), demonstrating that this distinctive chromosomal structure (henceforth, C11.2) corresponds to the driving region of IM62 LG11. The region of Cent728 hybridization on each non-C11.2 chromosome was flanked by arrays of typically pericentromeric retrotransposons (Fig. 1C and fig. S2C) (18). This pattern suggests that Cent728 is, if not the centromere-specifying DNA repeat, a marker for centromeric chromosomal regions. Although we cannot yet determine whether the molecular mechanism of *Mimulus* drive is strictly centromeric (5) and whether the duplication and expansion of Cent728 arrays is causal, this association is consistent with the genetic evidence for centromeric drive (13, 15).

We examined metaphase chromosomes from nearly isogenic lines (NILs) containing heterozygous introgressions of *M. guttatus* *D* in a largely *M. nasutus* genetic background (13). Both strong Cent728 arrays from IM62 C11.2 appear present in the NILs (Fig. 1D and fig. S2D), which

Division of Biological Sciences, University of Montana, Missoula, MT 59812, USA.

*To whom correspondence should be addressed. E-mail: lila.fishman@mso.umt.edu

†Present address: Program in Neuroscience, Harvard Medical School, Boston, MA 02115, USA.